

Investigation on Fracture Behavior of Grade 91 Steel at 300–550 °C

B. Shashank Dutt, M. Nani Babu, G. Shanthi, A. Moitra, and G. Sasikala

(Submitted September 25, 2017; in revised form June 5, 2018; published online October 30, 2018)

The fracture toughness (J_{1c}) of modified 9Cr-1Mo (P91 or Grade 91) steel was evaluated in the temperature range 300–550 °C. The yield strength and ultimate tensile strength values were observed to decrease with test temperatures. The ductility (% uniform elongation and post-necking elongation) was minimum in the temperature range 350–400 °C. From J - R curves established at 300, 350, 400, 450, 500, and 550 °C, fracture toughness (J_{1c}) and tearing modulus were determined at different loading rates of 0.01, 0.05 and 0.1 mm/s. For all the loading rates, J_{1c} values decreased in the temperature range 300–450 °C, followed by an increase in fracture toughness up to 550 °C. These trends in tensile and fracture properties can be attributed to the influence of dynamic strain aging.

Keywords dynamic strain aging, fracture toughness, tearing modulus, tensile properties

1. Introduction

Grade 91 (P91 or modified 9Cr-1Mo) steel is the material selected for steam generator components (SG) of Indian fast breeder reactor (Ref 1). In addition to fast breeder reactors, this steel is used for steam water systems of power plants and petrochemical industries. The steam generators of Indian nuclear reactors are subjected to operating temperatures between 370 and 550 °C. The fracture properties of P91 steel at these operating temperatures are required for assessing the structural integrity of SG components. The present investigation has been undertaken to characterize the fracture properties in the temperature range 300–550 °C.

Previous studies with respect to 9Cr-1Mo and P91 (or T91) steels have been carried out for various mechanical properties including tensile, low cycle fatigue, and fracture toughness (Ref 2–10). In this class of steels (Ref 5–9), it was reported that tensile and low cycle fatigue properties were influenced by dynamic strain aging (DSA). Kishore et al. (Ref 6) mentioned that DSA occurred in modified 9Cr-1Mo steel in the temperature range 200–450 °C. The manifestations of DSA with respect to tensile properties for various materials have been examined (Ref 11). Previous investigations reported that fracture toughness of various steels including P91 steel and austenitic stainless steels was influenced by DSA (Ref 10, 12, 13).

The authors (Ref 10) have previously reported that fracture toughness of P91 steel was reduced due to DSA. The authors have previously investigated (Ref 10) fracture properties for limited (25, 380, and 550 °C) number of test temperatures.

B. Shashank Dutt, M. Nani Babu, G. Shanthi, A. Moitra, and G. Sasikala, Metallurgy and Materials Group, Indira Gandhi Centre for Atomic Research, Kalpakkam 603 102, India. Contact e-mail: shashank@igcar.gov.in.

These three test temperatures are not sufficient enough to describe the effect of DSA on fracture behavior. In this investigation, test temperatures (300, 350, 400, 450, 500, and 550 °C) were considered in the close intervals (50 °C) to illustrate the DSA effects. In addition to test temperatures, the effect of loading rates (0.01, 0.05, and 0.1 mm/s) on fracture properties has been studied. In this investigation room temperature (RT) tests were not carried out for both tensile and fracture toughness testing, considering no significant effect of DSA on mechanical properties at RT.

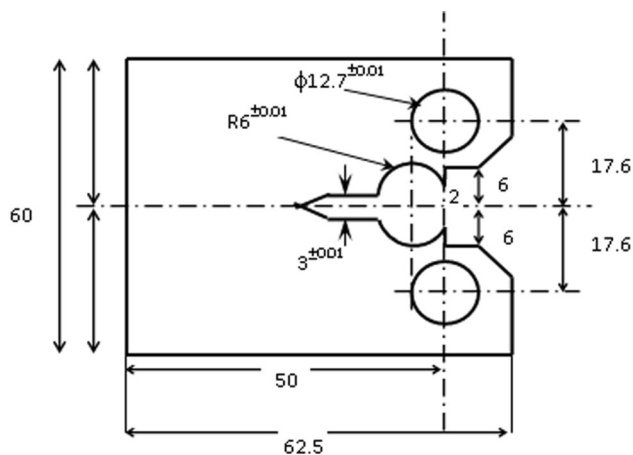
2. Experimental

The steel for this investigation was supplied in normalized (1040 °C, 60 min) and tempered (760 °C, 60 min) condition, and the chemical composition is mentioned in Table 1. From the plate, tensile specimens were fabricated having 28 mm gauge length and 4 mm gauge diameter as per ASTM E8 (Ref 14) standard. The specimen blanks for tensile testing were obtained in the rolling direction of the plate. The tensile tests were carried out in a screw-driven tensile testing machine fitted with high-temperature furnace. The tensile tests were carried out at temperatures of 300, 350, 400, 450, 500, and 550 °C at a strain rate of $1.2 \times 10^{-4} \text{ s}^{-1}$, and for all the test temperatures, three (3) specimens were tested. For all the test temperatures, specimens were heated in the furnace and soaked at test temperature for 1 h before application of tensile loads. The temperatures for all the tests were controlled within ± 2 °C. The load–elongation curves were monitored and recorded by digital data acquisition system.

Compact tension (CT) specimens (20 mm thickness and 50 mm width) were fabricated as per ASTM E 1820 (Ref 15) specifications. The schematic of CT specimen is shown in Fig. 1. The CT specimens were subjected to pre-cracking and side grooving for determination of J - R curves. The initial crack lengths (a_0) after pre-cracking were between 29 and 30 mm. The crack length after pre-cracking was targeted corresponding to crack length-to-width ratio (a/W) between 0.59 and 0.60. The pre-cracking was carried out at room temperature (RT) using resonant fatigue machine by subjecting the CT specimens under

Table 1 Chemical composition (wt.%)

C	Mn	Si	Ni	P	S	Cr	Mo	V	Nb	N	Fe
0.10	0.45	0.22	0.21	0.01	0.002	9.09	0.99	0.20	0.07	0.047	Bal.

**Fig. 1** Schematic of CT specimen

fatigue loading by stress intensity factor (K) in decreasing mode. The initial frequency of load cycle was ~ 100 Hz and loading range of 10-5 kN was applied. After pre-cracking the CT specimens were side-grooved to 20% net depth (2 mm deep groove on either surface). The J tests were carried out in a 50 ton servo-hydraulic machine having automated test control and data acquisition system. The experimental setup for fracture testing is shown in Fig. 2. The J tests were carried out for test temperatures 300, 350, 400, 450, 500, and 550 °C, and for all the test temperatures duplicate tests were carried out. The temperatures for all the tests were controlled within ± 2 °C. For all the test conditions, specimens soaked at test temperature for 1 h before the start of J tests at various displacement rates. For all test temperatures, fracture tests were done at load line displacement rates of 0.01, 0.05, and 0.1 mm/s.

The load (P) and load line displacement (LLD) data were recorded, and direct current potential drop (DCPD) device was used for online determination of crack length. The LLD was monitored using crack-opening displacement gauges. The tested specimens were heat-tinted (400 °C) and then pulled to fracture (room temperature). The initial (a_0) and final crack lengths (a_f) were optically determined by nine-point average method, and it was verified that the crack length values obtained from DCPD were in close agreement to the optically measured crack lengths. The fracture surfaces were examined in scanning electron microscope (SEM). From the fractographs, stretch zone width (SZW) measurements were carried out for all the test conditions. An average of 20 readings was considered for SZW measurements. The microstructures (optical and SEM) of the specimens prepared from fractographs for all test temperatures were observed. The microstructures were observed after polishing and etching with Vilella's reagent.

3. Results

The microstructure (SEM) after fracture tested at 300 °C is shown in Fig. 3. The microstructure revealed tempered martensite with prior austenite grain boundaries and lath boundaries. The microstructure revealed uniform distribution of precipitates. No significant changes in microstructure (optical and SEM) were observed after tensile and fracture testing at all the test temperatures, including the steel in as-received (normalized and tempered) condition.

During tensile testing, no serrations were observed in the stress-strain curves for this steel at all test temperatures. The yield strength and ultimate tensile strength values are plotted in Fig. 4(a). The strength values were observed to decrease with test temperatures. The ductility (% uniform elongation) was (Fig. 4b) minimum at 400 °C. The post-necking elongation (Fig. 4c) values were minimum in the temperature range 350-400 °C. From the true stress versus true strain curves, strain-hardening behavior was analyzed based on the equation ($\sigma = K(\epsilon)^n$). The strain-hardening exponent (n) values are plotted in Fig. 5. The n (Fig. 5) values were observed to increase in the temperature range 300-400 °C, followed by decrease in these values up to 550 °C.

From the load, load line displacement, and crack length values, J - Δa (or J - R) curves were determined as per ASTM 1820 (Ref 15). For the initial crack blunting line (Eq 1), ASTM E1820 specifies a minimum constant (M) value of 2.

$$J = M\sigma_f(\Delta a) \quad (\text{Eq 1})$$

where σ_{YS} = yield strength (YS), σ_f = flow stress = (YS + UTS)/2, UTS = ultimate tensile strength, Δa = crack extension, M = blunting line equation constant = 2 as per ASTM 1820.

From the J - Δa curves, fracture toughness (J_{1c}) values determined for all test temperatures and loading rates are plotted in Fig. 6. The tearing ($T = (\frac{E}{\sigma_{YS}})^2 (\frac{dJ}{da})$) modulus (corresponding to dJ/da values at 1 mm) for all test temperatures and loading rates are shown in Fig. 7. The J_{1c} values were observed to decrease in the temperature range 300-400 °C, followed by increase in fracture toughness up to 550 °C. The J_{1c} values for all test temperatures and loading rates satisfied the ASTM 1820 (Ref 15) validity criterion ($B > 10J_{1c}/\sigma_Y$). (B = thickness, σ_Y = flow stress). The tearing modulus values (Fig. 7) were minimum at 400 °C, followed by increase in tearing resistance up to 550 °C, for all the loading rates. From Fig. 6 and 7, it is clear that crack initiation resistance (fracture toughness) and tearing resistance show similar trends. The minimum in fracture toughness (Fig. 6) and post-necking elongation (Fig. 4c) occurred in similar temperature range (350-450 °C). Similar trends in ductility and fracture resistance were observed for similar type of steel by authors previously (Ref 10).

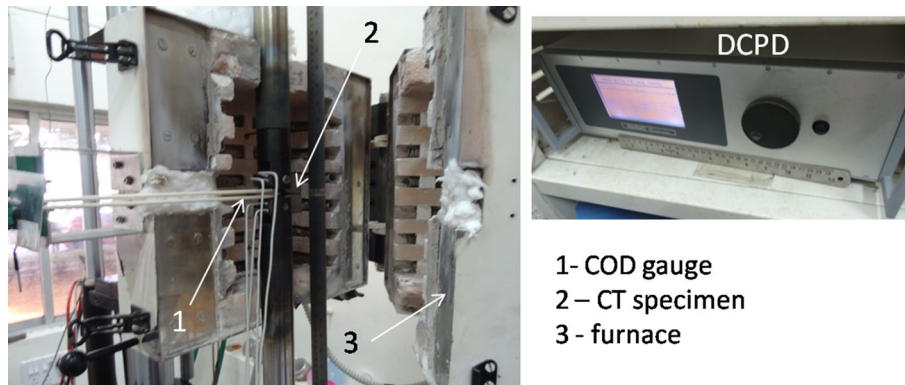


Fig. 2 Experimental setup for fracture testing

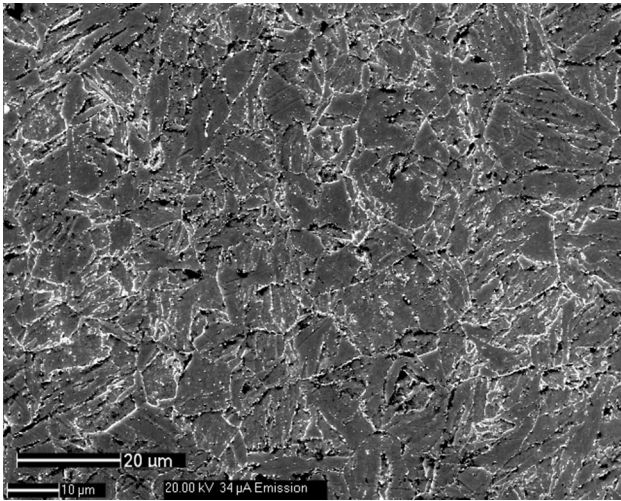


Fig. 3 Microstructure of P91 steel tested at 300 °C

The stretch zone width values for all test temperatures and loading rates are plotted in Fig. 8. No significant changes in SZW values were observed in the test temperature range 300-450 °C, for all loading rates. The SZW values were comparatively higher at 550 °C for all loading rates. The J values for all test conditions (temperatures and loading rates), corresponding to SZW (J_{SZW}), were determined by substitution of $SZW = \Delta a$ in Eq 1. The J_{SZW} values (Table 2) for all test conditions were lower than the fracture toughness (J_{Ic}) values.

The fractographs of specimens fracture tested at 300 and 400 °C are shown in Fig. 9(a) and (b). The fractographs revealed dimples, indicating ductile fracture. At 400 °C, the fractograph (Fig. 9b) revealed coarser dimples, and this temperature corresponded to minimum in fracture toughness.

It is widely reported for various steels that ductile fracture occurs by nucleation, growth, and coalescence of voids. For steels having various second-phase particles or precipitates as in the present case of P91 steel, void nucleation is expected predominantly at second-phase particles only, and by particle-matrix decohesion process (Ref 16). It may also be noted that the total energy to fracture includes the energy for nucleation, growth and coalescence of voids. In this steel possessing semi-coherent precipitates with higher interface strength, it is expected that the energy for nucleation would be substantial as compared to energy for void growth. In this backdrop, the

coarser dimple size may not be associated with higher fraction of energy, and thus may not be the rate controlling factor toward fracture. Further, the DSA is expected to induce negative strain rate sensitivity (Ref 5, 6), i.e., increase in strain rate would be associated with lowering of the flow stress. The higher strain rate associated with the void growth kinetics also expected to lower the flow stress requirement due to the DSA effect and could lead to early coalescence, instead of a delayed process.

From Fig. 9(b), considering spherical shape, radius of dimples was approximately 10 μm . The presence a few (spherical shaped) oxide particles (approximate size 3-4 μm) were observed in the fractograph (Fig. 9b). For P91 steels, previous investigators (Ref 17) have reported that $M_{23}C_6$ precipitates (spherical shape) were in the size range 25-150 nm (diameter). It can be noted that for fractograph at this particular magnification (1000 \times) and resolution (10 μm), the presence or absence of precipitates was not possible to be detected.

In this investigation, the oxide particles are not the primary void nucleating sites. These oxide particles were observed at very few pockets on the fracture surface. The precipitates are the predominant sites for nucleation of voids. In an investigation on the effect of various heat treatments on the microstructure and mechanical properties of P91 steel (Ref 18), it was reported that various carbide precipitates acted as sites for void nucleation. In this investigation, similar void nucleation mechanism was applicable.

4. Discussion

The results of this investigation can be compared to other investigations as follows. It is widely reported that Grade 91 steel has tempered martensite (metastable) microstructure with main precipitates as $M_{23}C_6$ (Cr rich) and MX (M = V, Nb, Cr; X = C, N) types. Previous investigations (Ref 17) for this grade of steel have reported that the microstructure of this steel is stable (resistance to coarsening of precipitates) in the temperature range 500-550 °C, for aging durations up to 1000 h. It was reported (Ref 19) that microstructure of modified 9Cr-1Mo steel was stable (martensite lath morphology retained) after annealing in the temperature range 500-600 °C. Baek et al. (Ref 20) concluded that the microstructure of modified 9Cr-1Mo steel was stable after aging at 600 °C for 50,000 h. In this investigation, the fracture and tensile tests were completed

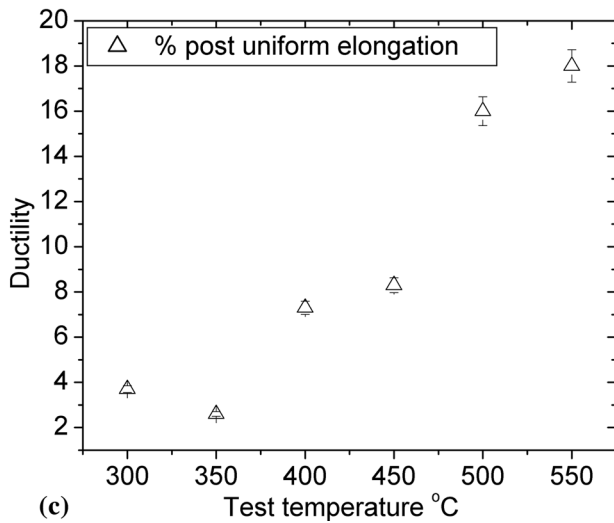
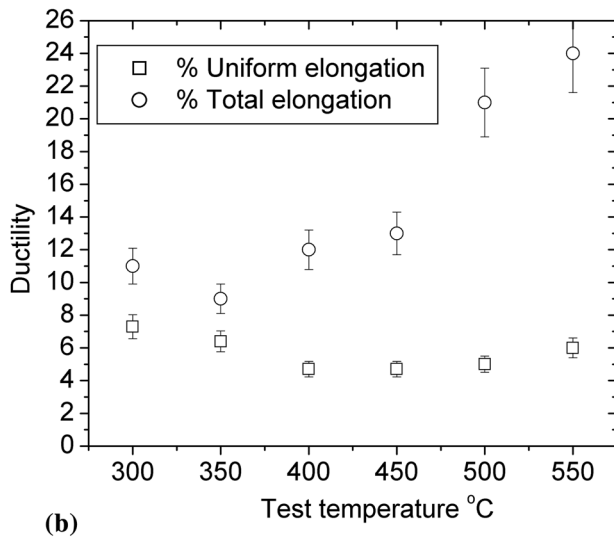
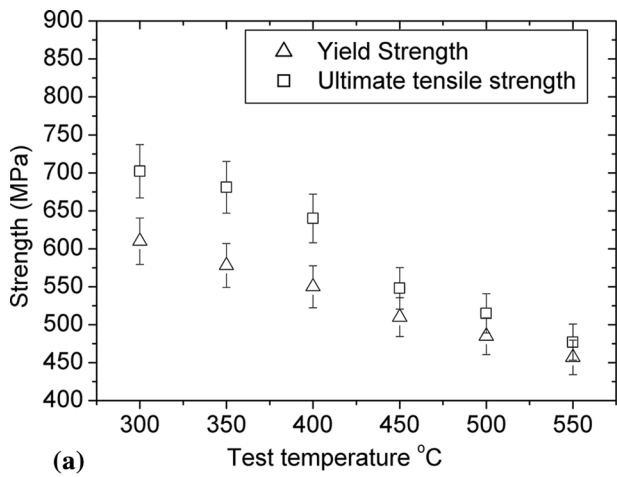


Fig. 4 (a-c) Tensile properties tested at various temperatures (a) strength (b) total and uniform elongations and (c) post necking elongation

within 10 h (maximum) durations, and based on previous studies (Ref 17-20), it can be inferred that no significant changes in microstructure occur in this steel for these test conditions.

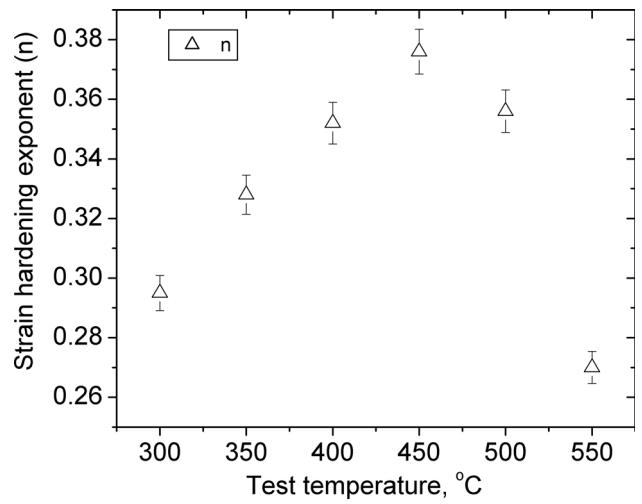


Fig. 5 Strain-hardening exponent (n) in the temperature range 300-550 °C

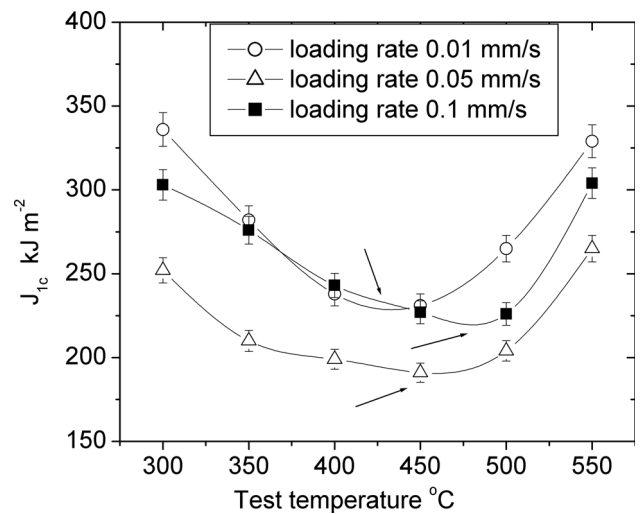


Fig. 6 Fracture toughness (J_{1c}) results at different temperatures and loading rates

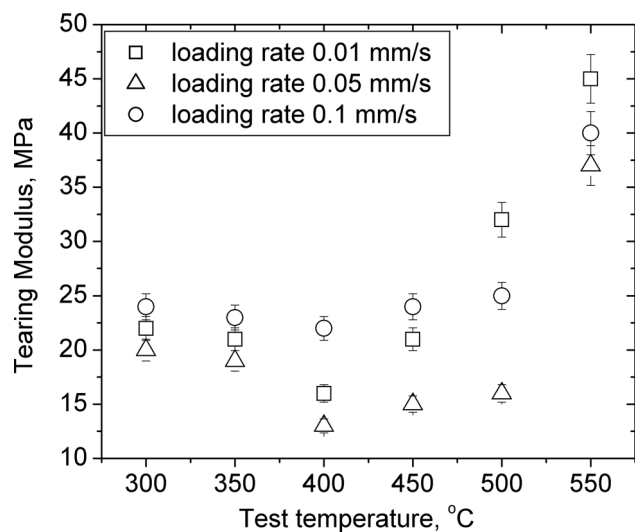


Fig. 7 Tearing modulus at different temperatures and loading rates

The tensile properties in this report are within the accepted limits of the minimum strength values for this class of steels (Ref 21) for fusion reactors and for sodium-cooled (Indian) fast reactor (Ref 1). For various steels including Grade 91 steel, it was reported (Ref 2-12) that DSA occurs due to interaction between the moving dislocations and solute atoms. During DSA the solute atoms having sufficient mobility, interact with the moving dislocations to form solute atmospheres and higher stresses are required for dislocations to break away from the solute atmosphere.

For this (P91) class of steels (Ref 4-6), the manifestation of DSA in the form of serrations in stress-strain curves were observed. In this investigation, serrations in the stress-strain curves were not observed. The manifestations (other than serrations) of DSA (Ref 11) include (a) negative strain rate sensitivity, (b) peak in flow stress, (c) minimum in ductility, and (d) peak in strain-hardening values. Previous investigators (Ref 5-10, 22) have reported only some manifestations of DSA, for various steels. The authors have previously (Ref 10) reported that absence of serrations does not rule out the occurrence of DSA. The authors (Ref 10) have previously reported (a) marginal decrease in ductility with test temperatures and (b) decrease in fracture toughness due to DSA. Kishore et al (Ref 6) reported the tensile properties of modified 9Cr-1Mo steel, tested at various temperatures and strain rates. DSA (Ref 6) was manifested by (a) maxima in ultimate tensile strength, (b) minima in ductility, and (c) negative strain rate sensitivity. The

modified 9Cr-1Mo steel (Ref 6) tested at 450 °C and after tempering at 550 °C was reported with persistent negative strain rate sensitivity, in the absence of serrations. For austenitic stainless steel, previous researchers (Ref 22) have reported that in the absence of serrations other indications of DSA included (a) anomalies in work hardening and (b) yield point transients on strain rate jump tests. It was reported (Ref 8, 9) that during low cycle fatigue testing of P91 steel, in the absence of serrations in the plastic portions of stress strain hysteresis loops,

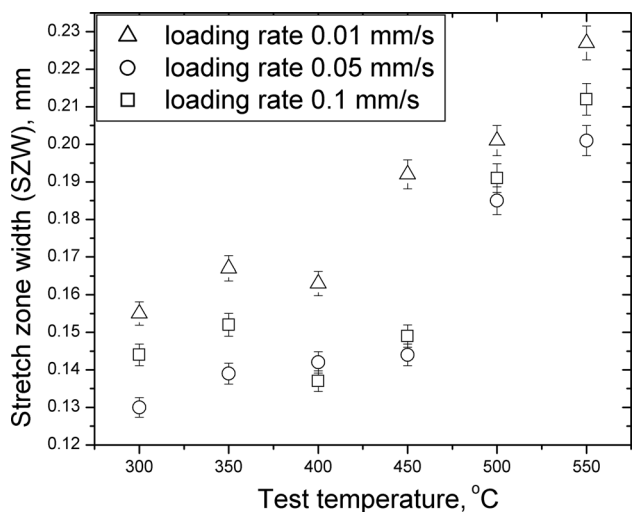
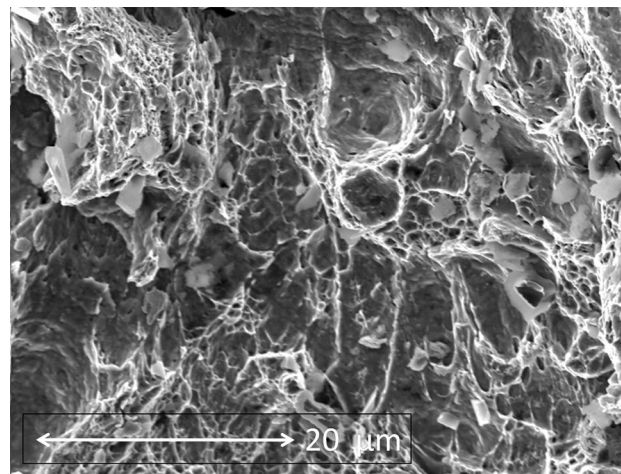
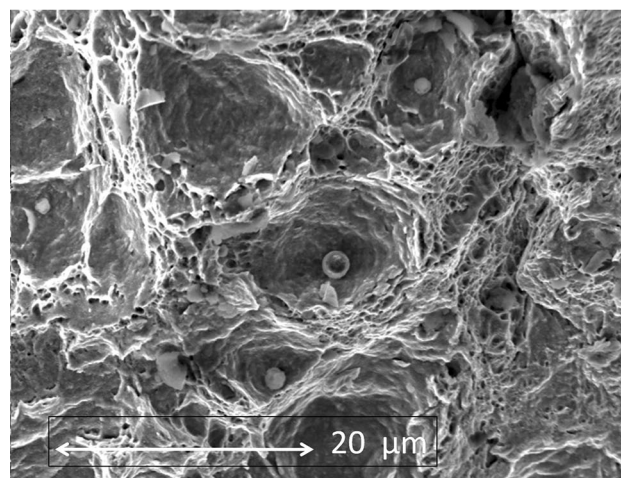


Fig. 8 Stretch zone width values at different temperatures



(a)



(b)

Fig. 9 (a, b) Fractographs of specimens tested at (a) 300 and (b) 400 °C

Table 2 $J (J_{szw})$ values corresponding to SZW

Test temperature, °C	J_{szw} , kJ/m ² (error ± 5 kJ/m ²)		
	Loading rate 0.01, mm/s	Loading rate 0.05, mm/s	Loading rate 0.1, mm/s
300	236	194	211
350	221	152	160
400	200	173	167
450	159	166	121
500	186	155	142
550	212	146	132

DSA can be confirmed by negative temperature dependence of half-life plastic strain amplitude.

Keller et al (Ref 7) reported the experimental analysis of DSA for modified T91 martensitic steel, tensile-tested in the temperatures from 100 to 450 °C at strain rates in the range 10^{-5} - 10^{-3} s⁻¹. DSA was reported (Ref 7) in the temperatures between 150 and 450 °C. The test conditions (temperatures between 150 and 450 °C) corresponding to the absence of serrations was reported (Ref 7). In a study (Ref 5) on the effect of DSA on the tensile and fracture properties of P91 steel, DSA and serrated flow were reported to occur between 250 and 350 °C and strain rate of 10^{-4} s⁻¹. In the temperature range from 250 to 350 °C, serrations were not observed (Ref 5) at strain rates of 10^{-5} and 10^{-3} s⁻¹. In this investigation the strain rate was $\sim 10^{-4}$ s⁻¹ and serrations were absent. In previous studies for similar (P91) steel tested at strain rate of 10^{-4} s⁻¹ and different temperature ranges (150-450 °C), serrations were absent (Ref 7). Hence, from the previous investigations (Ref 5-10, 22), it can be inferred that serrations occur for a particular test conditions, and in the absence of serrations, other manifestations (Ref 11) are applicable to confirm the occurrence of DSA.

In this investigation (a) minimum in % uniform elongation (Fig. 4b), (b) minimum in post-necking elongation (Fig. 4c), and (c) peak in strain-hardening exponent (n) (Fig. 5) observed are in agreement with previously reported (Ref 11) manifestations of DSA. Similar trends (minimum in ductility and maximum n values) were reported by other investigators for P91 steels (Ref 5, 6) tested at different temperatures and corresponding to strain rates of approximately 10^{-4} s⁻¹. In a previous study on the tensile deformation of 9Cr-1Mo steel (Ref 2), negative strain rate sensitivity, ductility minima, and maxima in work-hardening rate (θ) were reported. Keller et al (Ref 23) reported minima in fracture strain and maxima in strain-hardening exponent (n) for T91 steel tested from 100 to 450 °C (strain rate 10^{-4} s⁻¹). Hence it can be summarized that in this work the tensile properties were influenced by DSA.

For various steels, the activation energy during DSA is determined by Eq 2:

$$\dot{\epsilon} = A \exp(-Q/RT) \quad (\text{Eq 2})$$

where the dependence of strain rate ($\dot{\epsilon}$) on temperatures (T, K) are considered and Q is the action energy. To understand the mechanism for dynamic strain aging under different loading rates, activation energy was calculated by plotting the effective strain rate at crack tip ($\dot{\epsilon}$) (from the loading rates) with inverse of temperatures ($1000/T, T$ in K). The crack tip strain rate was calculated (Ref 24) based on Eq 3:

$$\dot{\epsilon} = (1.455)^n \frac{\Delta_L}{a h_3(a/w, n)} \quad (\text{Eq 3})$$

where the equivalent crack tip strain rate ($\dot{\epsilon}$) was calculated from the loading rates (Δ_L), crack length (a), specimen width (w), and strain-hardening exponent (n). The crack tip strain rate (Eq 3) was derived for plane strain condition, based on fully plastic solutions (Ref 25) for CT specimens and application of limit load analysis (Ref 26) under gross yielding conditions. In this investigation, n values (Fig. 5) varied between 0.29 and 0.38 for various temperatures. For Eq 3, $h_3(a/w, n)$ is geometry-dependent function, and for CT specimen (crack length-to-width ratio of 0.6.) in Ref 24, a constant value of $h_3 = 1.852$ was considered for this function. In this investigation, an

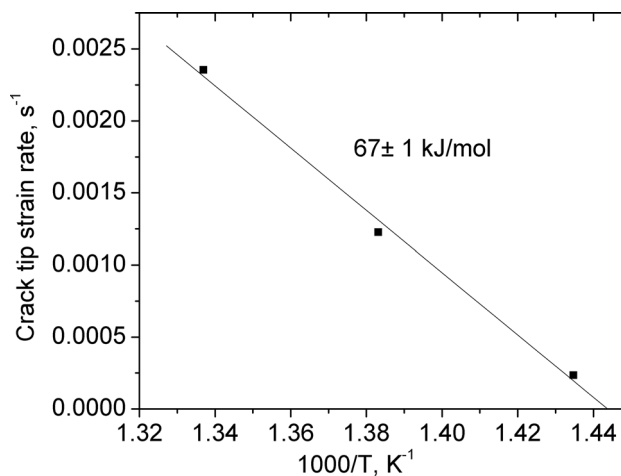


Fig. 10 Plot for determination of activation energy

approximate value of 1.8 was considered for $h_3(a/w, n)$ function, based on similarity in geometries (CT specimen) and similar crack length-to-width (a/W) ratio (0.6). In this study, estimated (Fig. 10) crack tip strain rates varied between 10^{-3} and 10^{-4} s⁻¹. In the previous investigation (Ref 24), for load line displacement rate of 1 mm/min, estimated crack tip strain rate was 2.0×10^{-3} s⁻¹.

In the previous (Ref 24) study, the minimum in fracture toughness corresponded to the absence of serrations. Previous investigators (Ref 5) estimated activation energy based on minimum in ductility. In this investigation, minimum in ductility (Fig. 4b and c) and fracture toughness (Fig. 6) occurred in the temperature range 350-450 °C. The strain rates were considered based on minimum values of fracture toughness in the temperature range 400- 475 °C and plotted as shown in Fig. 10. The activation energy was $\sim 67 \pm 1$ kJ/mol. The activation energies reported for this class of steels can be summarized as follows. For 9Cr-1Mo steels (Ref 2, 3), the activation energies were 83 and 86 KJ/mol. These studies (Ref 2, 3) attributed DSA to carbon alloying element. It was also reported that for P91 steels (Ref 4) with different silicon contents (wt.%) the activation energy was in the range 64-80 KJ/mol, and the activation energies varied with silicon contents. For modified 9Cr-1Mo steels, the activation energies reported were 45 (Ref 6) and 58 (Ref 5) KJ/mol and nitrogen was the element causing DSA. The authors have previously (Ref 27) reported activation energy in the range 55-80 kJ/mol for similar steel subjected to fatigue crack growth studies. In this investigation, it can be summarized that the minimum activation energy (67 ± 1 kJ/mol) was within the acceptable limits in this class of steels to explain DSA, considering that the activation energies reported (Ref 4) for Grade 91 class of steels vary with chemical composition. Similar mechanism (interstitial solute elements) can be applicable to Grade 91 steel in this study.

Previous investigators (Ref 28, 29) have reported thermodynamic (MatCalc and Thermo-Calc) and kinetics (Dictra)-based simulations for evolution of precipitates in this class of steels. Paul et al (Ref 17) mentioned that some carbonitride (MX) precipitates were not fully dissolved in austenite during normalization. In this investigation, Thermo-Calc (2016) was used to estimate the equilibrium composition of austenite (FCC) at normalization temperature (1050 °C, before cooling)

Table 3 Estimated composition (wt.%) of austenite (1050 °C) phase by Thermo-Calc

C	Mn	Si	Ni	Cr	Mo	V	Nb	N	Fe
0.098	0.45	0.22	0.21	9.07	0.99	0.14	0.011	0.025	88.7

and mentioned in Table 3. The calculations were performed under single-point equilibrium conditions for austenite phase. The estimated volume fraction of austenite was $\sim 99\%$, under the equilibrium condition corresponding to normalizing temperature (1050 °C). However, as previous experimental studies (Ref 17, 18) characterizing the microstructures have indicated, after normalization and tempering treatments, carbon and nitrogen are depleted due to precipitation of various phases (carbides and carbonitrides).

Various researchers have mentioned that decrease in fracture toughness occurred due to dynamic strain aging. In this work, decrease in J_{1c} and tearing modulus was observed in the temperature range 300–400 °C. Similar trends in fracture toughness (test temperatures 25, 380 and 550 °C) were observed for this class of steel by the authors previously (Ref 10). It can be noted that numerical variations in the range of SZW values in this investigation (0.13–0.22 mm) in comparison with previous (Ref 10) work (0.10–0.19 mm) were not significant. Marengo (Ref 13) reported fracture toughness of different pressure vessel steels and 304L stainless steel. For 304L stainless steel (Ref 13), no specific correlation between SZW, fracture toughness, and test temperatures were observed. In this investigation, no significant changes in SZW values were observed in the temperature range 300–450 °C. At 550 °C, higher SZW values can be explained based on higher plasticity at this temperature.

The above results have shown that in the temperature range of 350–450 °C, there is a dip in fracture toughness which has been attributed to the DSA effect. From Fig. 6, it can be observed that for loading rates of 0.01, 0.05, and 0.1 mm/s, the corresponding temperatures for the minimum J_{1c} values were 424, 450 and 475 °C, respectively. The estimated crack tip strain rates varied between 10^{-3} and 10^{-4} s^{-1} . The minimum in fracture toughness occurred at higher temperatures at higher strain rates. Similar observations in other materials also have been attributed to DSA (Ref 24, 30, 31). In this investigation, minimum in ductility (Fig. 4b and c), peak in strain-hardening (Fig. 5), and minimum in fracture toughness (Fig. 6) were observed in the temperature range 350–450 °C. The combined effect DSA and strain rate on the fracture resistance was more pronounced at loading rate of 0.05 mm/s. The mechanism responsible for DSA has been evaluated through correlating the crack tip strain rate as function of temperature. The activation energy found to be $\sim 67 \pm 1 \text{ kJ/mole}$ indicating that the interstitial diffusion could be the responsible for DSA. Hence it can be summarized that the fracture properties of P91 steel at all loading conditions were influenced by DSA.

5. Conclusions

The fracture behavior of Grade 91 steel has been studied in the temperature range 300–550 °C. The fracture toughness and tearing modulus values were minimum at 400 °C. The tensile

and fracture properties were influenced by dynamic strain aging. The presence of DSA can be confirmed by the decrease in strength, decrease in % uniform elongation, increase in strain-hardening exponent, and decrease in fracture toughness in the temperature range 300–400 °C.

References

1. A.K. Bhaduri and K. Laha, Development of Improved Materials for Structural Components of Sodium-Cooled Fast Reactors, *Proc. Eng.*, 2015, **130**, p 598–608
2. B.K. Choudhary, K.B.S. Rao, and S.L. Mannan, Effects of Strain Rate and Temperature on Tensile Deformation and Fracture Behaviour of Forged Thick Section 9Cr-1Mo Ferritic Steel, *Int. J. Press. Vessels Pip.*, 1994, **58**, p 151–160
3. B.K. Choudhary, Influence of Strain Rate and Temperature on Serrated Flow in 9Cr-1Mo Ferritic Steel, *Mater. Sci. Eng. A*, 2013, **564**, p 303–309
4. A.K. Roy, P. Kumar, and D. Maitra, Dynamic Strain Ageing of P91 Grade Steels of Varied Silicon Content, *Mater. Sci. Eng. A*, 2009, **499**, p 379–386
5. P. Verma, G.S. Rao, P. Chellapandi, G.S. Mahobia, K. Chattopadhyay, N.C.S. Srinivas, and V. Singh, Dynamic Strain Ageing, Deformation and Fracture Behavior of Modified 9Cr-1Mo Steel, *Mat. Sci. Eng. A*, 2015, **621**, p 39–51
6. R. Kishore, R.N. Singh, and B.P. Kashyap, Effect of Dynamic Strain Ageing on the Tensile Properties of a Modified 9Cr-1Mo Steel, *J. Mater. Sci.*, 1997, **32**, p 437–442
7. C. Keller, M.M. Margulies, and I. Guillot, Experimental Analysis of the Dynamic Strain Ageing for a Modified T91 Martensitic Steel, *Mater. Sci. Eng. A*, 2012, **536**, p 273–275
8. A. Nagesha, M. Valsan, R. Kannan, K.B.S. Rao, and S.L. Mannan, Influence of Temperature on the Low Cycle Fatigue Behaviour of a Modified 9Cr-1Mo Ferritic Steel, *Int. J. Fatigue*, 2002, **24**, p 1285–1293
9. S.L. Mannan and M. Valsan, High-Temperature Low Cycle Fatigue, Creep-Fatigue and Thermomechanical Fatigue of Steels and Their Welds, *Int J Mech Sc*, 2006, **48**, p 160–175
10. B.S. Dutt, M.N. Babu, S. Venugopal, G. Sasikala, and A.K. Bhaduri, Effect of Test Temperature on Fracture Toughness of Modified 9Cr-1Mo Steel, *Mater. Sci. Technol.*, 2011, **27**, p 1527–1533
11. P. Rodriguez, Serrated Plastic Flow, *Bull. Mater. Sci.*, 1984, **6**, p 653–664
12. K.G. Samuel, O. Gossman, and H. Huthmann, Temperature Dependence of Fracture Toughness (J-R curves) of a Modified Type 316 L Austenitic Stainless Steel, *Int. J. Pressue Vessels Pip.*, 1990, **41**, p 59–74
13. A.A. Marengo and J.E.P. Ipinia, Pressure Vessel Steel Fracture Toughness in the Regime from Room Temperature to 400 °C, *Nucl. Eng. Des.*, 1996, **167**, p 215–222
14. ASTM E8/E8M-16a, Standard Test Methods for Tension Testing of Metallic Materials, ASTM International, West Conshohocken, PA, (2016). <https://www.astm.org>
15. ASTM E1820-17a, Standard Test Method for Measurement of Fracture Toughness, ASTM International, West Conshohocken, PA, (2017). <https://www.astm.org>
16. A. Moitra, P.R. Sreenivasan, S.L. Mannan, and V. Singh, Ductile-Brittle Transition Temperatures and Dynamic Fracture Toughness of 9Cr-1Mo Steel, *Mater. Met Trans A*, 2005, **36**, p 2957–2965

17. V.T. Paul, S. Saroja, and M. Vijayalakshmi, Microstructural Stability of Modified 9Cr-1Mo Steel During Long Term Exposures at Elevated Temperatures, *J. Nucl. Mater.*, 2008, **378**, p 273–281
18. C. Pandey, A. Giri, and M.M. Mahapatra, Evolution of Phases in P91 Steel in Various Heat Treatment Conditions and Their Effect on Microstructural Stability and Mechanical Properties, *Mater. Sci. Eng. A*, 2016, **664**, p 58–74
19. W.B. Jones, C.R. Hills, and D.H. Polonis, Microstructural Evolution of Modified 9Cr-1Mo steel, *Met. Trans. A*, 1991, **22**, p 1049–1058
20. J.H. Baek, S.H. Kim, C.B. Lee, and D.H. Hahn, Mechanical Properties and Microstructural Evolution of Modified 9Cr-1Mo Steel After Long Term Aging for 50,000 h, *Met. Mater. Int.*, 2009, **15**, p 565–573
21. A.A.F. Tavasoli, Materials Design Data for Fusion Reactor, *J. Nucl. Mater.*, 1998, **258**, p 85–96
22. S.K. Ray, K.G. Samuel, and P. Rodriguez, Dynamic Strain Ageing in Type 316 Stainless Steel at 300 K, *Scr. Metall. Mater.*, 1992, **27**, p 271–276
23. C. Keller, M.M. Margulies, Z.H. Hamouche, and I. Guillot, Influence of the Temperature on the Tensile Behaviour of a Modified 9Cr-1Mo T91 Martensitic Steel, *Mater. Sci. Eng. A*, 2010, **527**, p 6758–6764
24. J.H. Yoon, B.S. Lee, Y.S. Oh, and J.H. Hong, Effects of Loading Rate and Temperature on J–R Fracture Resistance of an SA516-Gr.70 Steel for Nuclear Piping, *Int. J. Press. Vessels Pip.*, 1999, **76**, p 663–670
25. V. Kumar, M.D. German, and C.F. Shih, An Engineering Approach for Elastic-Plastic Fracture Analysis, EPRI report NP-1931 (1981), p 1–234. (<https://www.osti.gov/servlets/purl/6068291>)
26. J.G. Merkle and H.T. Corten, A J Integral Analysis for the Compact Specimen Considering Axial Force as Well as Bending Effects, *J. Press. Vessel Technol.*, 1974, **96**, p 286–292
27. M.N. Babu, G. Sasikala, B.S. Dutt, S. Venugopal, S.K. Albert, A.K. Bhaduri, and T. Jayakumar, Investigation on Influence of Dynamic Strain Ageing on Fatigue Crack Growth Behaviour of Modified 9Cr–1Mo Steel, *Int. J. Fatigue*, 2012, **43**, p 242–245
28. B.S.S. Prasad, V.B.R. Kumar, and K.C.H. Kumar, Numerical Simulation of Precipitate Evolution in Ferritic-Martensitic Power Plant Steels, *CALPHAD*, 2012, **36**, p 1–7
29. J. Hald, Metallurgy and Creep Properties of New 9-12%Cr Steels, *Steel Res*, 1996, **67**, p 369–374
30. I.S. Kim and S.S. Kang, Dynamic Strain Aging in SA-508-Class 3 Pressure Vessel Steel, *Int. J. Press. Vessels Pip.*, 1995, **62**, p 123–129
31. J.W. Kim and I.S. Kim, Investigation of Dynamic Strain Aging in SA 106 Gr.C Piping Steel, *Nucl Eng Des*, 1997, **172**, p 49–59